WPJET1-PR(17) 17592

D Tegnered et al.

Gyrokinetic simulations of particle transport in pellet fuelled JET discharges

Preprint of Paper to be submitted for publication in
Plasma Physics and Controlled Fusion

This work has been carried out within the framework of the EUROfusion Consortium and has received funding from the Euratom research and training programme 2014-2018 under grant agreement No 633053. The views and opinions expressed herein do not necessarily reflect those of the European Commission.

Gyrokinetic simulations of particle transport in pellet fuelled JET discharges

D. Tegnered[1], H. Nordman[1], M. Oberparleiter[1], P. Strand[1], L. Garzotti[2], I. Lupelli[2], C. M. Roach[2], M. Romanelli[2], M. Valovič[2] and JET Contributors*

[1] *Chalmers University of Technology, SE-412 96 Gothenburg, Sweden.*

[2] *CCFE, Culham Science Centre, Abingdon, OX14 3DB, UK.*

[*] *See the author list of "Overview of the JET results in support to ITER" by X. Litaudon et al. to be published in Nuclear Fusion Special issue: overview and summary reports from the 26th Fusion Energy Conference (Kyoto, Japan, 17-22 October 2016)*

E-mail: `tegnered@chalmers.se`

Abstract

Pellet injection is a likely fuelling method of reactor grade plasmas. When the pellet ablates, it will transiently perturb the density and temperature profiles of the plasma. This will in turn change dimensionless parameters such as a/L_n, a/L_T and plasma β. The microstability properties of the plasma then changes which influences the transport of heat and particles. In this paper, gyrokinetic simulations of a JET L-mode pellet fuelled discharge are performed. The Ion Temperature Gradient/Trapped Electron (ITG/TE) mode turbulence is compared at the time point when the effect from the pellet is the most pronounced with a hollow density profile and when the profiles have relaxed again. Linear and nonlinear simulations are performed using the gyrokinetic code GENE including electromagnetic effects and collisions in a realistic geometry in local mode. Furthermore, global nonlinear simulations are performed in order to assess any nonlocal effects. It is found that the positive density gradient has a stabilizing effect that is partly counteracted by the increased temperature gradient in the this region. The effective diffusion coefficients are reduced in the positive density region region compared to the intra pellet time point. No major effect on the turbulent transport due to nonlocal effects are observed.

1. Introduction

Pellet injection is the likely fuelling method of reactor grade plasmas. Unlike when using fuelling by gas puffing, injecting a pellet into the plasma temporarily perturbs both the density and temperature profiles, resulting in changes in dimensionless parameters such as a/L_n, a/L_T, collisionality and plasma β. The density profile may become hollow

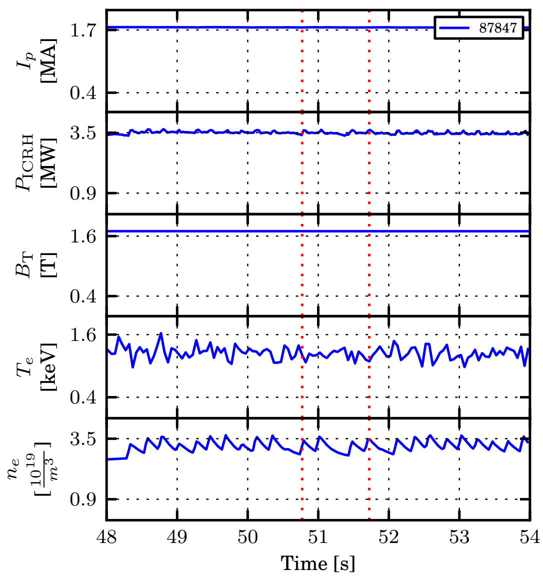

Figure 1: Time evolution of the plasma current, ICRH power, toroidal magnetic field, electron temperature on the magnetic axis, and line averaged core electron density during the flat top. Time points of analysis indicated with dotted lines.

with regions of positive density gradients and steeper negative density gradients on the outside of the pellet ablation peak. This will in turn affect microstability and transport properties of the discharge. Hydrogen pellet injection experiments were performed during the JET hydrogen campaign in 2014. The target were L-mode ICRH-heated hydrogen plasmas. The diagnostic set-up was optimised to measure the post pellet evolution of the density profile with high spatial resolution and the pellet injection frequency (14 Hz) was chosen with respect to sampling time of the Thomson scattering measurements (50 ms) to exploit a 'stroboscopic' effect and virtually enhance the time resolution of the profile measurement. Accurate equilibrium reconstruction and Gaussian process regression fits [1] of the kinetic profiles were performed to provide the basis for gyrokinetic analysis of the pellet cycle and characterise the transport properties of these pellet fuelled plasmas. The discharge under study here is no. 87847 with a toroidal magnetic field of 1.7 T, a plasma current of 1.75 MA and 3.45 MW of ICRH power. The time evolution of the plasma current, ICRH power, and magnetic field, along with the electron temperature and density are shown in Figure 1. Microstability analysis of a typical MAST pellet fuelled discharge was previously performed in [2] where a stabilization of all modes in the negative a/L_n (positive density gradient) region was found. The quasilinear gyrokinetic code QuaLiKiz [3] has been previously used to study the microturbulence during the L to H transition which is also associated with hollow density profiles, it was shown that the TE mode was stabilized and that the particle flux was highly sensitive to the sign of R/L_n [4].

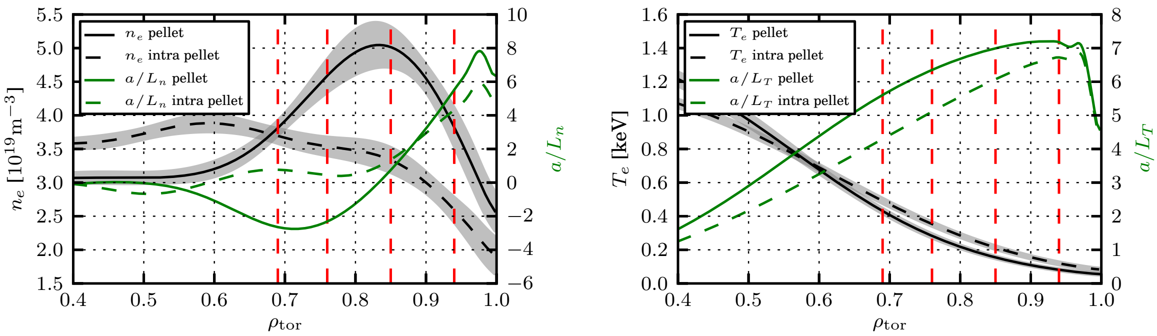

(a) Density profiles (b) Temperature profiles

Figure 2: Profiles of density and temperature at the two time points. Dashed lines indicate radial positions of the gyrokinetic analysis.

The discharge is analysed at several radial positions around the density peak and at several time points after the injection of the pellet. The focus is on the time point when the density peak from the ablation pellet is the largest, $t = 0.0042\,\mathrm{s}$ after the pellet injection, referred to as 'pellet'. The results are compared and contrasted to the time point when the peak is relaxed again at 0.034 s, referred to as 'intra pellet'. The profiles of temperature and density and the resulting normalized gradient scale lengths are shown in Figure 2 and the discharge parameters are given in Table 1. The gyrokinetic code GENE [5, 6] is used to study the transport due to Ion Temperature Gradient/Trapped electron mode (ITG/TE) [7, 8, 9, 10, 11, 12, 13] turbulence. These modes are the main source of particle transport in the core of tokamak plasmas [14]. Both linear and nonlinear simulations are performed in a flux tube domain, including finite β effects and collisions in realistic geometry. We note that the collisionality is high in the present discharge and have included collisionless simulations in order to connect our results to more reactor relevant conditions. Since the pellet causes the density to vary significantly over a rather narrow radial region, the possible role of nonlocal phenomena is also studied in nonlinear global simulations in a reduced physics description including only electrostatic effects and adiabatic electrons. Because of this, the global simulations cannot describe particle transport or the TE mode, but a comparison of heat fluxes to similar local simulations can nevertheless indicate whether there are any nonlocal effects. Since this is a hydrogen discharge, simulations are also run with deuterium in order to assess any effects going to reactor relevant isotopes. The paper is organized as follows. In section 2 the discharge parameters and simulation setup are introduced, followed by the linear GENE results in section 3. In section 4 the local nonlinear results are presented and in section 5 follows the study of the isotopic effect. In section 6 global effects are investigated and finally in section 7 we have the concluding remarks.

ρ_{tor}	t [s after pellet]	n [$10^{19}/\text{m}^3$]	T [keV]	a/L_T	a/L_n	η	ν_{ei} [c_s/a]	β [%]	q	$\hat{s}$
0.69	0.0042	3.81	0.43	5.60	-2.64	-2.12	1.39	0.20	1.61	1.32
0.69	0.034	3.69	0.49	4.29	0.77	5.57	1.05	0.22	1.60	1.34
0.76	0.0042	4.59	0.28	6.35	-2.32	-2.74	3.73	0.16	1.86	1.64
0.76	0.034	3.54	0.35	5.11	0.42	12.2	1.89	0.15	1.85	1.66
0.85	0.0042	5.01	0.15	7.00	0.74	9.46	13.00	0.10	2.30	2.20
0.85	0.034	3.34	0.21	6.08	1.36	4.47	4.74	0.09	2.30	2.22
0.94	0.0042	3.83	0.08	7.16	5.50	1.30	34.44	0.04	3.01	3.42
0.94	0.034	2.60	0.12	6.71	4.33	1.55	11.36	0.04	3.01	3.43

Table 1: Discharge parameters of the four radial positions and two time points. n is the density, $T = T_e = T_i$ is the temperature, $a/L_T = a/L_{T_e} = a/L_{T_i}$ is the normalized temperature gradient, a/L_n is the normalized density gradient, $\eta = L_n/L_T$, ν_{ei} is the electron-ion collision rate, β is the electron β, q is the safety factor and $\hat{s}$ is the magnetic shear.

2. GENE simulation setup

GENE solves the nonlinear gyrokinetic Vlasov equation coupled with Maxwell's equations in order to find the distribution functions of the species, $f\left(\mathbf{R}, v_\parallel, \mu, t\right)$, the electrostatic potential, $\phi(\mathbf{x}, t)$ and the parallel components of the magnetic vector potential and magnetic field, $A_\parallel(\mathbf{x}, t)$ and $B_\parallel(\mathbf{x}, t)$. It is a Eulerian δf-type code where the coordinate system is aligned to the background magnetic field with x as the radial coordinate, y as the binormal coordinate, and z as the parallel coordinate. Collisions are modelled using a linearised Landau-Boltzmann collision operator [15]. Magnetic fluctuations perpendicular and parallel to the magnetic field are included in all simulations. A numeric equilibrium reconstructed using the EFIT++ code [16] is used in either a local, flux-tube domain or global domain. In the simulation, $T_i = T_e$ is assumed, and impurities are not included in the simulations. Fast particles and rotation are not expected to play an important role in this low-β, ICRH heated discharge and are not included.

3. Linear results

For the linear GENE simulation, a resolution typically used is $\left[n_x, n_z, n_{v_\parallel}, n_\mu\right] = [16, 64, 32, 24]$. In cases where subdominant modes are discussed an eigenvalue solver is used, otherwise an initial value solver is used. The linear eigenvalues in SI units at $k_y\rho_s = 0.3$ as a function of ρ_{tor} for the pellet and intra pellet time points are shown in Figure 3. The growth rates at this wave number are reduced in the positive density gradient region $0.62 < \rho_{\text{tor}} < 0.8$ compared to the intra pellet time point, for both collisional and collisionless cases. The eigenvalue spectra at four radial positions around the pellet ablation density peak are shown in Figure 4 at the pellet and intra pellet time points. The four radial points are at $\rho_{\text{tor}} = 0.69$ and $\rho_{\text{tor}} = 0.76$ in the positive gradient region, $\rho_{\text{tor}} = 0.85$ at the peak density and at $\rho_{\text{tor}} = 0.94$ in the negative gradient

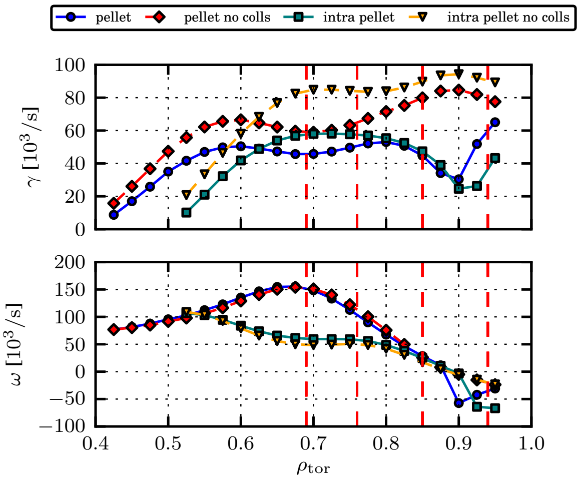

Figure 3: Linear eigenvalues for $k_y\rho_s = 0.3$ as a function of $\rho_{\rm tor}$ at the two different time points, with and without collisions.

region. The eigenvalue spectra is dominated by the ITG mode for $k_y\rho_s < 1.2$ in the four cases as indicated by the positive real frequency. In the positive density gradient region, $\rho_{\rm tor} = 0.69$ and $\rho_{\rm tor} = 0.76$, the pellet growth rates are slightly reduced in normalized units for $k_y\rho_s < 0.7$ compared to the intra pellet time point in the collisional case. In the collisionless case the effect is more pronounced. Primarily without collisions, there is a subdominant TE mode which also has reduced growth rates at the pellet time point. This stabilization is likely due to more favourable trapped particle drifts.[17] At $\rho_{\rm tor} = 0.85$ and $\rho_{\rm tor} = 0.94$ the ITG mode is instead destabilized at the pellet time point, with and without collisions. The same is true for the TE mode which is only destabilized without collisions.

In Figure 5 scans in temperature and density gradients are shown at the pellet and intra pellet time points, for $k_y\rho_s = 0.3$ and $\rho_{\rm tor} = 0.69$. The results are similar at $\rho = 0.76$ and at other wave numbers in the ITG wave number range. The pressure gradient as considered in the curvature and ∇B drifts is calculated self-consistently from the density and temperature gradients. In the a/L_T scan, the growth rate is reduced in the pellet case at similar a/L_T, with a greater reduction in the collisionless case. The ITG threshold is increased from $a/L_T \sim 1$ in the intra pellet case to $a/L_T \sim 3$ in the pellet case. In the a/L_n scan a reduction in growth rate is seen in the collisional case both going to large positive and negative density gradients, while in the collisionless cases a large value of a/L_n is destabilizing. At similar a/L_n the pellet time point is more unstable because of the higher a/L_T. Taken together, going from the intra pellet to the pellet time point there is a stabilizing effect due to negative a/L_n but a destabilizing effect due to an increase in a/L_T that partially undoes the stabilization, resulting in the growth rate spectra exhibited in Figure 4. A similar situation was seen at MAST with counteracting density and temperature gradients at the inside of the

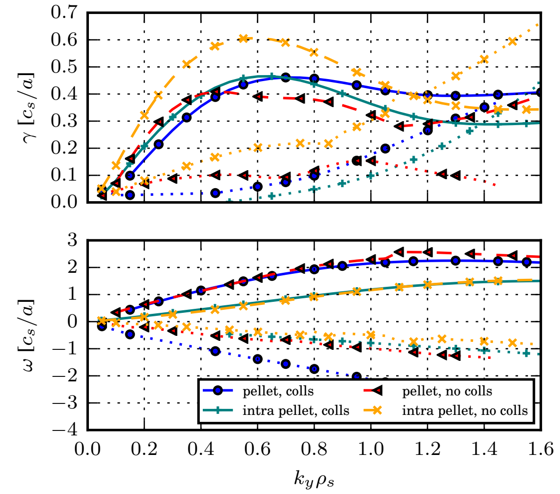

(a) $\rho_{\rm tor} = 0.69$

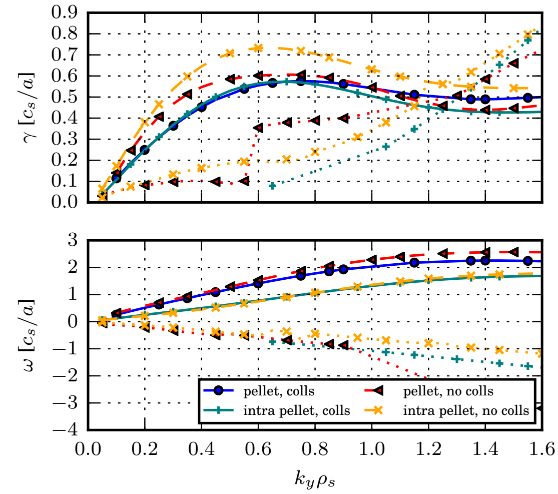

(b) $\rho_{\rm tor} = 0.76$

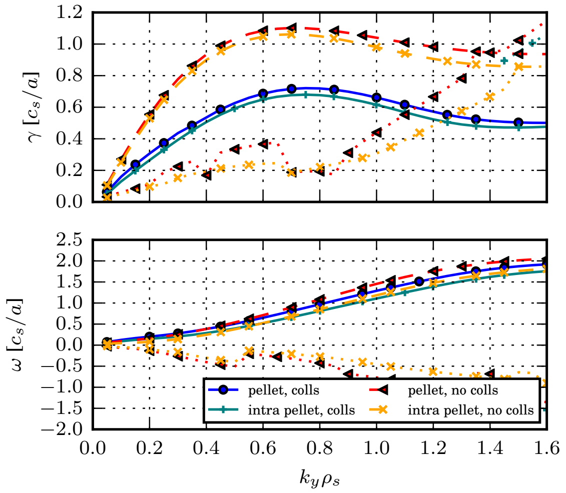

(c) $\rho_{\rm tor} = 0.85$

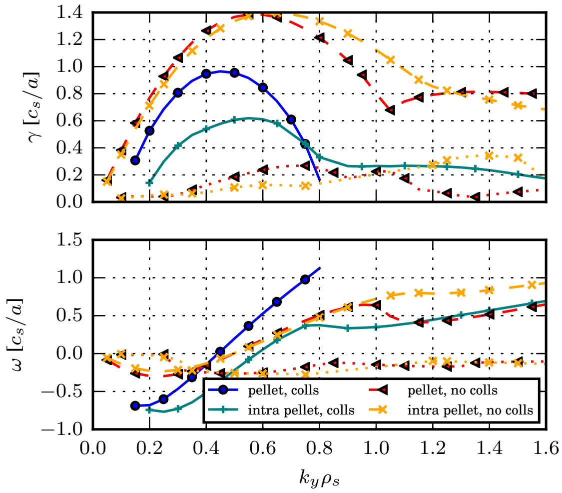

(d) $\rho_{\rm tor} = 0.94$

Figure 4: Eigenvalue spectra at the four radial distances at the two different time points, with and without collisions, TE mode dotted.

pellet ablation peak [18]. In previous gyrokinetic simulations in the positive gradient region at MAST, however, a complete stabilization of the ITG and TE modes in this wave number range was observed [2]. In that experiment, the observed reduction in the magnitude of $\eta_i = |L_{n_e}/L_{T_i}|$ going from the reference to the pellet profiles was however much larger in the positive density gradient region. The situation at MAST was also different close to the pellet density peak where the ITG growth rates were reduced and the micro tearing mode became dominant. This was due to an increase in β from 2.5 % to 4.5 %, whereas at JET β increases only slightly from 0.09 % to 0.10 %, and the

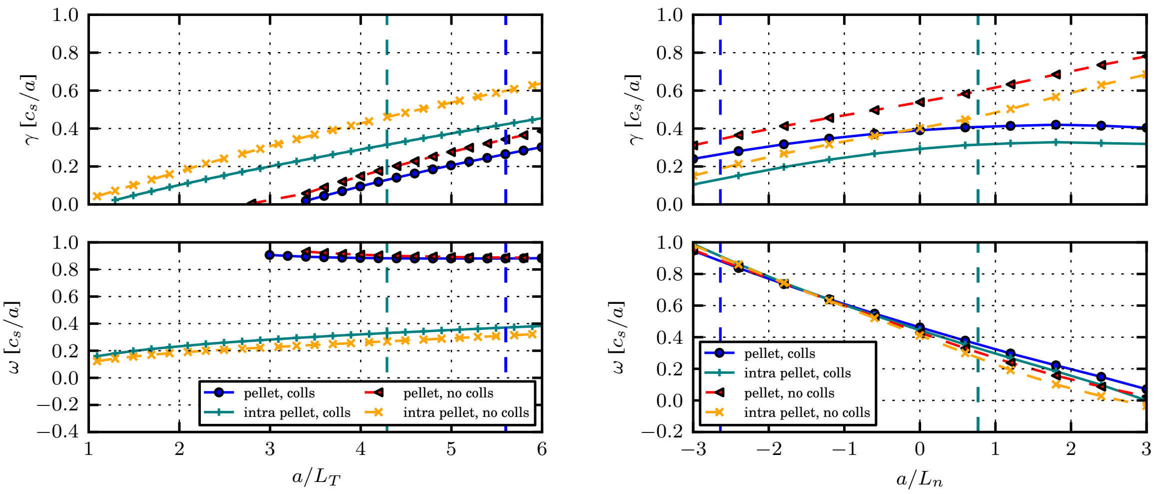

(a) (b)

Figure 5: Eigenvalue scans at $k_y\rho_s = 0.3$ in temperature and density gradients at the two different time points at $\rho_{\mathrm{tor}} = 0.69$ with and without collisions. Vertical lines indicate the experimental density and temperature gradients at this radius.

effect from the increase of η_i is more important here, destabilizing the ITG mode.

4. Nonlinear results

4.1. Flux-tube simulations

For the nonlinear local GENE simulations, a simulation domain in the perpendicular plane of 125 to 250 ion larmor radii in the poloidal direction and 110 to 240 in the radial direction was typically used, with a typical resolution of $\left[n_x, n_{k_y}, n_z, n_{v_\parallel}, n_\mu\right] = [144, 48, 32, 64, 16]$. The typical covered poloidal wave number range is $0.05 \leq k_y\rho_s \leq 2.4$. The four radial positions chosen for the nonlinear simulations are $\rho_{\mathrm{tor}} = 0.69$ and $\rho_{\mathrm{tor}} = 0.76$ in the negative a/L_n region, $\rho_{\mathrm{tor}} = 0.85$ close to the peak of the pellet ablation profile and $\rho_{\mathrm{tor}} = 0.94$ in the positive a/L_n region. In order to make a more straightforward comparison between the fluxes at different radial positions, the fluxes and resulting effective diffusion coefficients are shown in SI units.

In Figure 6a the particle fluxes and diffusion coefficients at these radial positions are shown for the collisional case. The particle flux is inwards on the inside of the pellet ablation peak and changes sign on the outside. The particle fluxes are of similar magnitude but with different sign on each side of the pellet ablation peak. There is a slight asymmetry with the larger fluxes being on the outside. In the negative a/L_n region the diffusion coefficients are lower just after the pellet than at the intra-pellet time. In the collisionless case, shown in Figure 6b, the inward particle pinch is stronger at both time points in the positive gradient region. A similar trend for negative a/L_n,

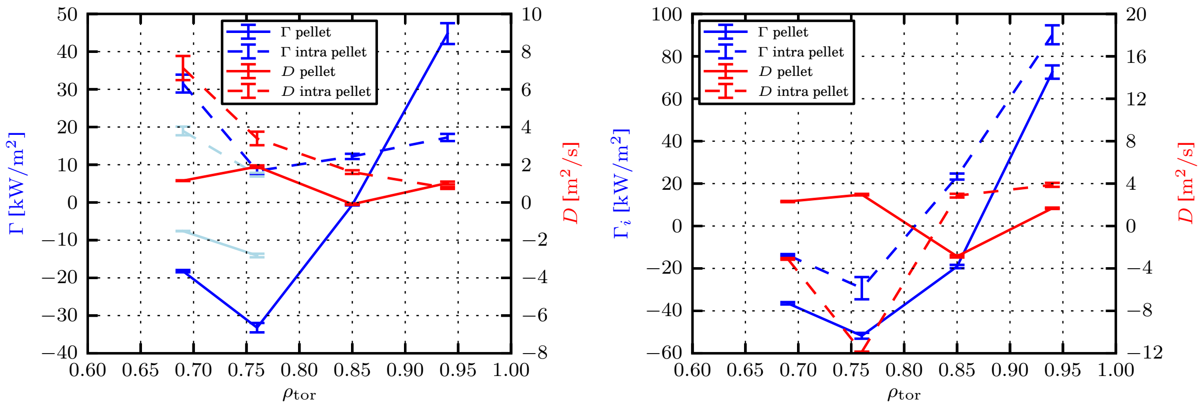

(a) Collisional case (b) Collisionless case

Figure 6: Nonlinear particle fluxes and effective diffusion coefficients. Light blue lines indicate the sensitivity to a 20% reduction in a/L_T.

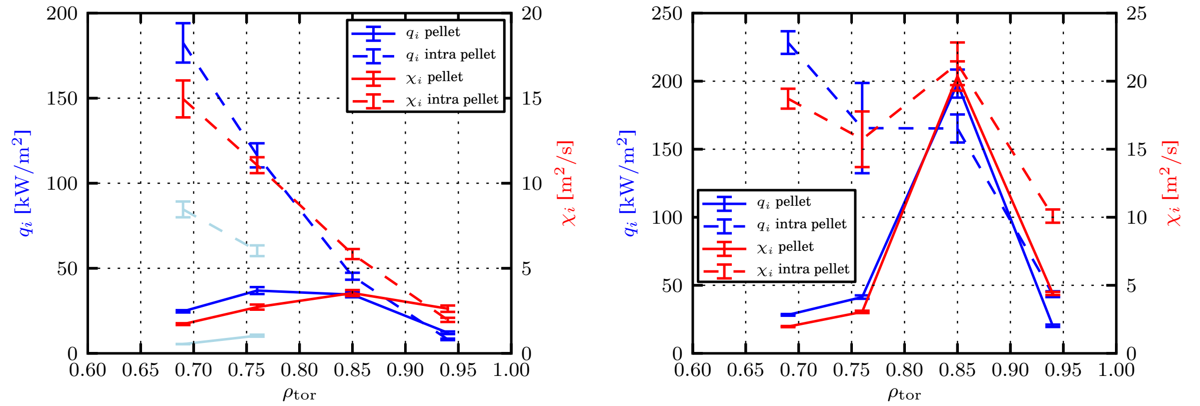

(a) Collisional case (b) Collisionless case

Figure 7: Nonlinear ion heat fluxes and effective heat diffusivities. Light blue lines indicate the sensitivity to a 20% reduction in a/L_T.

with a less inward particle flux as the collisionality increases, was found in [4]. At the intra pellet time point the flux has changed direction to inwards, compared to the outward flux at this time point in the collisional case. The magnitude of the effective particle diffusion coefficients are still smaller at the pellet time point compared to the intra pellet time point in the positive gradient region.

The nonlinear ion heat fluxes are shown in Figure 7. The outward heat fluxes are greatly reduced in the negative a/L_n radial range compared to the intra pellet case in both the collisional and collisionless cases, while they are more similar at the $\rho_{\rm tor} = 0.85$ and $\rho_{\rm tor} = 0.94$ positions. This, and the similar reduction in diffusion coefficients, is connected to the reduction in nonnormalized growth rates, as shown in Figure 3, in the

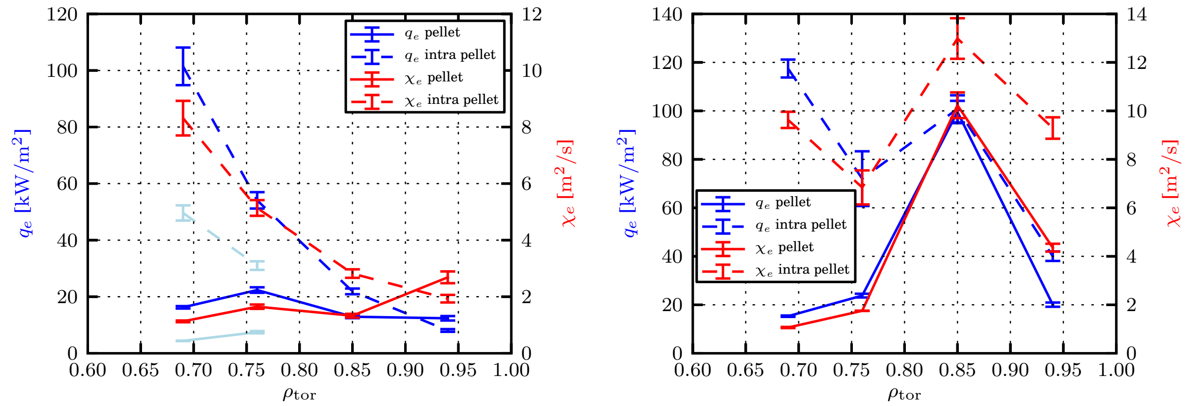

(a) Collisional case

(b) Collisionless case

Figure 8: Nonlinear electron heat fluxes and effective heat diffusivities.

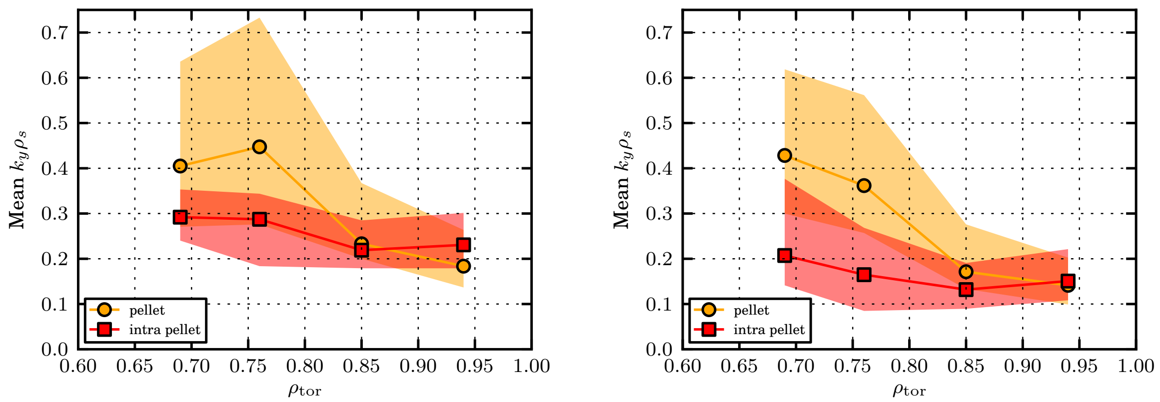

(a) Mean $k_y\rho_s$ of the ion particle flux, with collisions

(b) Mean $k_y\rho_s$ of the ion particle flux, without collisions

Figure 9: Mean $k_y\rho_s$ for the ion particle flux along with a measure of the width of the spectra.

positive gradient region. The electron heat fluxes, shown in Figure 8, follow the same trend as the ion heat fluxes.

In Figure 9 the ion particle flux weighted mean $k_y\rho_s$ is shown along with a measure of the width of the flux spectra. The width is taken as the range of wave numbers responsible for 25% of the flux over and under the indicated mean. In both the collisional and collisionless cases the mean wave number of the turbulence is lower in the intra pellet case in the negative R/L_n region, which is consistent with the larger heat fluxes at the intra pellet time point.

5. Comparison of H and D main ions

In JET, the confinement in the core region of ELMy H-mode plasmas has been observed to decrease with isotope mass, with $\chi_i \propto m^{0.73\pm0.4}$ [19]. However, in more recent L-mode JET discharges and in H-mode discharges in JT-60U and ASDEX Upgrade an improvement in confinement going from lower to higher hydrogen isotope masses have been observed [20, 21, 22]. This is in contrast to the gyro-Bohm scaling on turbulent transport which predicts $q_i \propto m_j^{1/2}$. This inconsistency has been called the isotope effect. Several explanations have been proposed, such as stronger zonal flows with heavier isotopes which reduces the turbulent transport [23]. In gyrokinetic modelling the effect from zonal flows have been shown to reduce the heat fluxes compared to the gyro-Bohm scaling for CBC parameters [24]. For an ITER scenario the interaction between ExB shear, zonal flows, magnetic geometry and electromagnetic effects has been shown to play a role in the explanation of the isotope effect on the particle and heat fluxes [25]. In global gyrokinetic simulations, it has been shown that GAMs also can play a role in the explanation of the isotope effect [26].

In the present modelling, the main ion isotope is changed from hydrogen to deuterium with unchanged density and temperature profiles. Finite β effects and collisions are included, as before. In species units, with $c_j = \sqrt{T_e/m_j} \propto m_j^{-1/2}$ and $\rho_j = \frac{c_j}{eB/m_j c} \propto \sqrt{m_j}$, the spectra are rather similar with the growth rates only slightly reduced in the deuterium case, as shown in Figure 10, with the strongest effect at $\rho_{\mathrm{tor}} = 0.69$. The difference vanishes for $k_y\rho_j < 0.6$ without collisions. This indicates that the fluxes should follow the gyro-Bohm scaling if no nonlinear effects differ between the hydrogen and deuterium simulations. This is verified with the nonlinear fluxes shown in Figure 11. Here, the fluxes are shown in species units, $Q_{gB_j} = c_j nT(\frac{\rho_j}{a})^2 \propto \sqrt{m_j}$ and $\Gamma_{gB_j} = c_j n(\frac{\rho_j}{a})^2 \propto \sqrt{m_j}$ so that any differences show the deviation from the gyro-Bohm scaling. For the particle fluxes, shown in Figure 11a, with a deuterium main ion the outward fluxes at the intra pellet time point are slightly reduced while the inward particle fluxes at the pellet time point are increased. The D and H heat fluxes, shown in Figure 11b are within the error bars. Zonal flow activity, as indicated by the average shearing rate $\left\langle \left\langle \left| \frac{d}{dx} v_{E\times B,y} \right|^2 \right\rangle_x^{1/2} \right\rangle_t$, is similar for hydrogen and deuterium.

6. Global simulations

For the global nonlinear simulations the electrons were treated in the adiabatic limit. Although particle transport and the TE mode cannot be described in this simplified physical description, a comparison to similar simulations in the local limit is nevertheless illuminating. The radial simulation domain covered $\rho_{\mathrm{tor}} = 0.505 - 0.995$ with a dampening buffer zone beyond $\rho_{\mathrm{tor}} = 0.945$, which is greyed out in the figure. The poloidal direction spanned 350 ion larmor radii. The grid was chosen as $\left[n_x, n_{k_y}, n_z, n_{v_\parallel}, n_\mu\right] = [768, 48, 64, 48, 32]$. The normalised gyroradius $\rho_* = \rho_i/a$ ranges

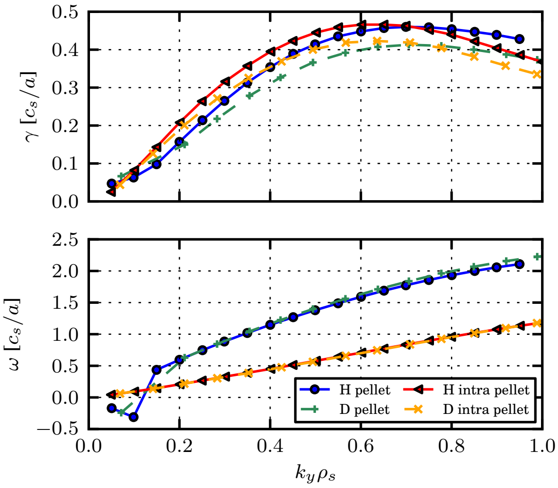

(a) $\rho_{\rm tor} = 0.69$

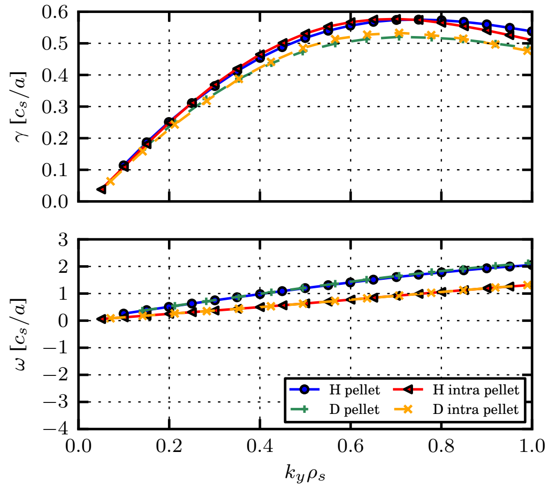

(b) $\rho_{\rm tor} = 0.76$

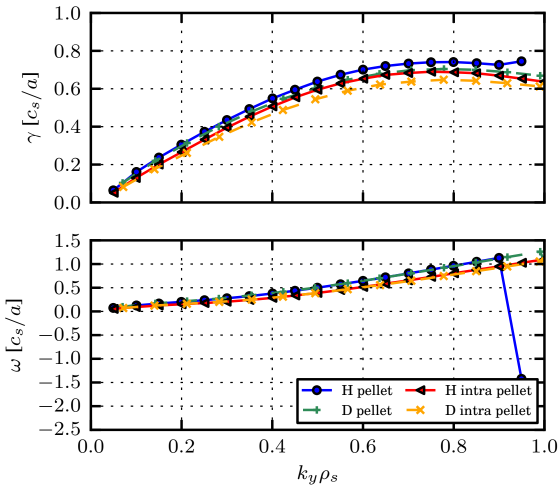

(c) $\rho_{\rm tor} = 0.85$

Figure 10: Eigenvalue spectra in species units at three radial distances with hydrogen and deuterium main ions.

between 1/600 and 1/1200 in the considered plasma region. Thus, we only expect that nonlocal phenomena can play a role for the pellet time point where the density gradient profile is peaked with a width of Δ_n and a $\rho_{*,eff} = \rho_i/\Delta_n$ of around 1/300 [27, 28].

We compare the heat flux from the global simulation for the pellet time point with local simulations with the same physics model at several radial positions in Figure 12. Qualitatively, i.e. in the shape of the heat flux profile, we find similarities with the local results with electrodynamic effects in Figure 7a but with an overall smaller level of flux. For $\rho_{\rm tor} < 0.7$ agreement between global and local simulations within the error bars is

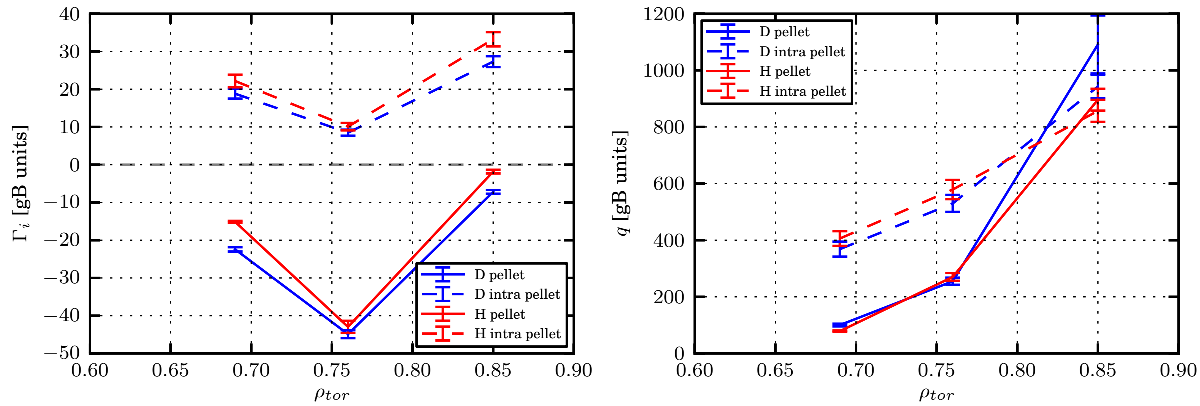

(a) Particle fluxes

(b) Heat fluxes

Figure 11: Particle and heat transport in species units at the pellet and intra pellet time points with hydrogen and deuterium main ions.

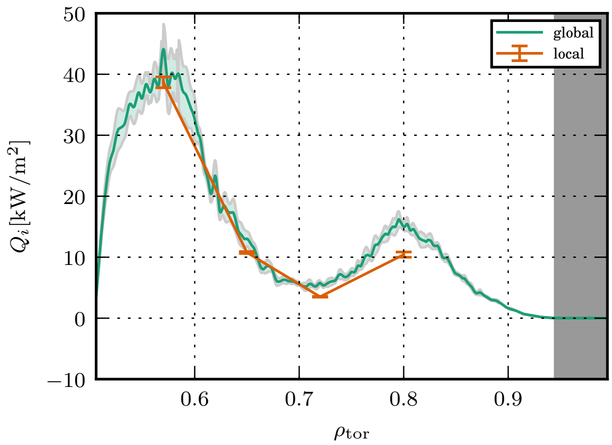

Figure 12: Radial turbulent ion heat flux at the pellet time point in global and local simulations with adiabatic electrons

found. At radial positions further out, however, a smaller heat flux is observed in the local simulations, in particular for $\rho_{\rm tor} = 0.80$.

In summary, we find that nonlocal effects do not seem to play a major role for this particular scenario and the previously presented flux-tube results are a reasonable approach for modelling turbulence after pellet injection in this JET discharge.

7. Conclusions

In this paper transport analysis of a pellet fuelled L-mode JET discharge has been performed using the gyrokinetic code GENE. Linearly it was shown that the dominating ITG-mode was slightly stabilized in normalized units on the inside of the pellet ablation peak compared to the intra pellet interval when the density gradients had relaxed. While the negative a/L_n was stabilizing, this was partially counteracted by the increase in a/L_T on the inside of the pellet ablation peak compared to the intra pellet gradients, resulting in similar growth rates. Nonlinearly, the particle fluxes on each side of the peak were slightly asymmetric with the larger fluxes being on the outside of the peak. This is a similar but smaller effect than was seen at MAST [2]. The effective diffusion coefficients were reduced compared to the intra pellet time point. In collisionless simulations, the particle fluxes were larger and more asymmetric around the peak, with stronger outward fluxes on the outside, but an inward flux at the top of the pellet ablation peak. The magnitude of the effective diffusion coefficients were still reduced compared to the intra pellet time point. In a comparison of hydrogen and deuterium plasma with with the same profiles as before, the particle fluxes only slightly deviated from the gyro-Bohm scaling. In global simulations no major effect on the turbulent transport due to nonlocal effects could be observed.

Acknowledgements

The simulations were performed on resources provided by the Swedish National Infrastructure for Computing (SNIC) at PDC Centre for High Performance Computing (PDC-HPC), on the HELIOS supercomputer system at Computational Simulation Centre of International Fusion Energy Research Centre (IFERC-CSC), Aomori, Japan, under the Broader Approach collaboration between Euratom and Japan, implemented by Fusion for Energy and JAEA, and at the Marconi supercomputer system, at Cineca, Casalecchio di Reno, Italy. This work was funded by a grant from The Swedish Research Council (C0338001). This work has been carried out within the framework of the EUROfusion Consortium and has received funding from the Euratom research and training programme 2014-2018 under grant agreement No 633053. The views and opinions expressed herein do not necessarily reflect those of the European Commission.

References

[1] MA Chilenski, M Greenwald, Y Marzouk, NT Howard, AE White, JE Rice, and JR Walk. Improved profile fitting and quantification of uncertainty in experimental measurements of impurity transport coefficients using gaussian process regression. *Nuclear Fusion*, 55(2):023012, 2015.

[2] L Garzotti, J Figueiredo, CM Roach, M Valovič, D Dickinson, G Naylor, M Romanelli, R Scannell, and G Szepesi. Microstability analysis of pellet fuelled discharges in mast. *Plasma Physics and Controlled Fusion*, 56(3):035004, 2014.

[3] C Bourdelle, X Garbet, F Imbeaux, A Casati, N Dubuit, R Guirlet, and T Parisot. A new gyrokinetic quasilinear transport model applied to particle transport in tokamak plasmas. *Physics of Plasmas (1994-present)*, 14(11):112501, 2007.

[4] B Baiocchi, C Bourdelle, C Angioni, F Imbeaux, A Loarte, and M Maslov. Transport analysis and modelling of the evolution of hollow density profiles plasmas in jet and implication for iter. *Nuclear Fusion*, 55(12):123001, 2015.

[5] http://genecode.org/.

[6] F Jenko, W Dorland, M Kotschenreuther, and BN Rogers. Electron temperature gradient driven turbulence. *Physics of Plasmas (1994-present)*, 7(5):1904–1910, 2000.

[7] BB Kadomtsev and OP Pogutse. Trapped particles in toroidal magnetic systems. *Nuclear Fusion*, 11(1):67, 1971.

[8] B Coppi and F Pegoraro. Theory of the ubiquitous mode. *Nuclear Fusion*, 17(5):969, 1977.

[9] W Horton Jr, D Choi, and WM Tang. Toroidal drift modes driven by ion pressure gradients. *Physics of Fluids (1958-1988)*, 24(6):1077–1085, 1981.

[10] PN Guzdar, L Chen, WM Tang, and PH Rutherford. Ion temperature gradient instability in toroidal plasmas. *Physics of Fluids (1958-1988)*, 26(3):673–677, 1983.

[11] F Romanelli. Ion temperature-gradient-driven modes and anomalous ion transport in tokamaks. *Physics of Fluids B: Plasma Physics (1989-1993)*, 1(5):1018–1025, 1989.

[12] H Biglari, PH Diamond, and MN Rosenbluth. Toroidal ion-pressure-gradient-driven drift instabilities and transport revisited. *Physics of Fluids B: Plasma Physics (1989-1993)*, 1(1):109–118, 1989.

[13] T Dannert and F Jenko. Gyrokinetic simulation of collisionless trapped-electron mode turbulence. *Physics of Plasmas (1994-present)*, 12(7):072309, 2005.

[14] Clemente Angioni, Emiliano Fable, M Greenwald, Mikhail Maslov, AG Peeters, H Takenaga, and Henri Weisen. Particle transport in tokamak plasmas, theory and experiment. *Plasma Physics and Controlled Fusion*, 51(12):124017, 2009.

[15] F Merz. *Gyrokinetic simulation of multimode plasma turbulence.* PhD thesis, Universitat Munster, 2008.

[16] LC Appel, GTA Huysmans, LL Lao, PJ McCarthy, DG Muir, ER Solano, J Storrs, D Taylor, W Zwingmann, et al. A unified approach to equilibrium reconstruction. In *Proceedings-33rd EPS conference on Controlled Fusion and Plasma Physics, pp. P–2.160*, 2006.

[17] CM Roach, JW Connor, and S Janjua. Trapped particle precession in advanced tokamaks. *Plasma physics and controlled fusion*, 37(6):679, 1995.

[18] M Valovič, K Axon, L Garzotti, S Saarelma, A Thyagaraja, R Akers, C Gurl, A Kirk, B Lloyd, GP Maddison, et al. Particle confinement of pellet-fuelled tokamak plasma. *Nuclear Fusion*, 48(7):075006, 2008.

[19] JG Cordey, B Balet, DV Bartlett, RV Budny, JP Christiansen, GD Conway, L-G Eriksson, GM Fishpool, CW Gowers, JCM De Haas, et al. Plasma confinement in jet h mode plasmas with h, d, dt and t isotopes. *Nuclear fusion*, 39(3):301, 1999.

[20] H. Urano, T. Takizuka, T. Fujita, Y. Kamada, T. Nakano, N. Oyama, and the JT-60 Team. Energy confinement of hydrogen and deuterium h-mode plasmas in jt-60u. *Nuclear Fusion*, 52(11):114021, 2012.

[21] H. Urano, T. Takizuka, N. Aiba, M. Kikuchi, T. Nakano, T. Fujita, N. Oyama, Y. Kamada, N. Hayashi, and the JT-60 Team. Hydrogen isotope effects on itg scale length, pedestal and confinement in jt-60 h-mode plasmas. *Nuclear Fusion*, 53(8):083003, 2013.

[22] M. Bessenrodt-Weberpals, F. Wagner, O. Gehre, L. Giannone, J.V. Hofmann, A. Kallenbach, K. McCormick, V. Mertens, H.D. Murmann, F. Ryter, B.D. Scott, G. Siller, F.X. Soldner, A. Stabler, K.-H. Steuer, U. Stroth, N. Tsois, H. Verbeek, and H. Zoohm. The isotope effect in asdex. *Nuclear Fusion*, 33(8):1205, 1993.

[23] T.S. Hahm, Lu Wang, W.X. Wang, E.S. Yoon, and F.X. Duthoit. Isotopic dependence of residual zonal flows. *Nuclear Fusion*, 53(7):072002, 2013.

[24] A Bustos, A Bañón Navarro, T Görler, F Jenko, and C Hidalgo. Microturbulence study of the isotope effect. *Physics of Plasmas*, 22(1):012305, 2015.

[25] J Garcia, T Görler, F Jenko, and G Giruzzi. Gyrokinetic nonlinear isotope effects in tokamak plasmas. *Nuclear Fusion*, 57(1):014007, 2016.

[26] AD Gurchenko, EZ Gusakov, P Niskala, AB Altukhov, LA Esipov, TP Kiviniemi, T Korpilo, DV Kouprienko, SI Lashkul, S Leerink, et al. The isotope effect in turbulent transport control by gams. observation and gyrokinetic modeling. *Plasma Physics and Controlled Fusion*,

58(4):044002, 2016.
[27] Z. Lin, S. Ethier, T. S. Hahm, and W. M. Tang. Size scaling of turbulent transport in magnetically confined plasmas. *Phys. Rev. Lett.*, 88:195004, Apr 2002.
[28] B. F. McMillan, X. Lapillonne, S. Brunner, L. Villard, S. Jolliet, A. Bottino, T. Görler, and F. Jenko. System size effects on gyrokinetic turbulence. *Phys. Rev. Lett.*, 105:155001, Oct 2010.